Integrated Imaging Methodology Detects Claudin-1 Expression in Premalignant Nonpolypoid and Polypoid Colonic Epithelium in Mice

Fa Wang, PhD[1], Xiyu Duan, PhD[2], Jing Chen, PhD[1], Zhenghong Gao, PhD[1], Juan Zhou, PhD[1], Xiaoli Wu, PhD[1], Tse-Shao Chang, MS[1], Miki Lee, MS[1], Gaoming Li, PhD[1], Asma Nusrat, MD[3], Rork Kuick, MA[4], Henry D. Appelman, MD[3] and Thomas D. Wang, MD, PhD[1,2,5]

OBJECTIVES: **Conventional colonoscopy with white light illumination detects colonic adenomas based on structural changes alone and is limited by a high miss rate. We aim to demonstrate an integrated imaging strategy that combines wide-field endoscopy and confocal endomicroscopy in real time to visualize molecular expression patterns *in vivo* to detect premalignant colonic mucosa.**

METHODS: **A peptide specific for claudin-1 is labeled with Cy5.5 and administrated intravenously in genetically engineered mice that develop adenomas spontaneously in the distal colon. Wide-field endoscopy is used to identify the presence of nonpolypoid and polypoid adenomas. Anatomic landmarks are used to guide placement of a confocal endomicroscope with side-view optics to visualize claudin-1 expression patterns with subcellular resolution.**

RESULTS: **Wide-field fluorescence images show peak uptake in colon adenoma at ~1 hour after systemic peptide administration, and lesion margins are clearly defined. Further examination of the lesion using a confocal endomicroscope shows dysplastic crypts with large size, elongated shape, distorted architecture, and variable dimension compared with normal. The mean fluorescence intensity is significantly higher for dysplasia than normal. Increased claudin-1 expression in dysplasia vs normal is confirmed *ex vivo*, and the binding pattern is consistent with the *in vivo* imaging results.**

DISCUSSION: **Wide-field endoscopy can visualize molecular expression of claudin-1 *in vivo* to localize premalignant colonic mucosa, and confocal endomicroscopy can identify subcellular feature to distinguish dysplasia from normal.**

SUPPLEMENTARY MATERIAL accompanies this paper at http://links.lww.com/CTG/A135, http://links.lww.com/CTG/A136, http://links.lww.com/CTG/A137, http://links.lww.com/CTG/A138, http://links.lww.com/CTG/A139, http://links.lww.com/CTG/A140, http://links.lww.com/CTG/A141, http://links.lww.com/CTG/A142, http://links.lww.com/CTG/A143, http://links.lww.com/CTG/A144, http://links.lww.com/CTG/A145, http://links.lww.com/CTG/A146, http://links.lww.com/CTG/A147, http://links.lww.com/CTG/A148, http://links.lww.com/CTG/A149

Clinical and Translational Gastroenterology 2020;11:e00089. https://doi.org/10.14309/ctg.0000000000000089

INTRODUCTION

Colorectal cancer (CRC) results in over 700,000 deaths per year globally, representing the third most common cause of cancer-related mortality worldwide (1). These numbers are expected to double over the next several decades as a result of a steady rise in obesity, an aging population, and a greater adoption of western diets (e.g., high fat and low fiber) in developing countries (2–4). More effective methods for early CRC detection are needed to address this growing health care burden. Colonoscopy is widely performed for cancer screening and has been shown to reduce overall CRC mortality (5). This wide-field imaging procedure is minimally invasive and can rapidly visualize large mucosal surface areas in real time to identify grossly visible polyps for resection. However, use of conventional white light illumination alone has limited diagnostic effectiveness. Tandem colonoscopy studies have shown >25% of all polyps are missed (6,7). Furthermore, up to 44% of all premalignant lesions are flat in appearance (8). Reports of "interval CRCs" that arise within 5 years after a "negative" colonoscopy are increasing (9,10).

Premalignant lesions express molecular targets well before structural changes become grossly apparent. This window of opportunity allows for more effective methods to detect adenomas that are nonpolypoid or subtle in appearance. Highly specific

[1]Division of Gastroenterology, Department of Internal Medicine, University of Michigan, Ann Arbor, Michigan, USA; [2]Department of Biomedical Engineering, University of Michigan, Ann Arbor, Michigan, USA; [3]Department of Pathology, University of Michigan, Ann Arbor, Michigan, USA; [4]Department of Biostatistics, University of Michigan, Ann Arbor, Michigan, USA; [5]Department of Mechanical Engineering, University of Michigan, Ann Arbor, Michigan, USA.
Correspondence: Thomas D. Wang, MD, PhD. E-mail: thomaswa@umich.edu.
Received March 19, 2019; accepted August 20, 2019; published online January 9, 2020

molecular probes, including antibodies, enzyme-activated probes, lectins, and peptides, are being developed that provide a biological basis for cancer detection (11–13). These probes are fluorescently labeled to generate high contrast for real-time visualization of overexpressed targets *in vivo*. Peptides can be administered in high concentrations to maximize target interactions and achieve rapid binding with minimal risk of toxicity. Previously, a peptide that binds specifically to the extracellular domain of claudin-1 was identified using phage display (14). Claudin-1 is a tight junction protein that maintains cell polarity and regulates paracellular transport and is a downstream target in the Wnt/β-catenin signaling pathway (15,16). Several studies have reported upregulation of claudin-1 in CRC (16–18).

Confocal endomicroscopy is an emerging imaging technique that can be used *in vivo* to collect histology-like images from the epithelium with subcellular resolution (19,20). This powerful method for optical sectioning uses a flexible fiber coupled to optics in a package with millimeter dimensions and can be used repetitively in small animals (19–21). These instruments were designed to interrogate tissues with an imaging depth up to several hundred microns and can be used to study tumor cell proliferation, migration, and invasion. Changes in molecular expression patterns can be visualized over time (19,20). Wide-field imaging methods can be combined with confocal endomicroscopy to first localize suspicious mucosal regions for more detailed investigation at much higher magnification. Here, we aim to demonstrate an integrated imaging strategy to target claudin-1 expression *in vivo* in normal and premalignant colonic epithelium. A peptide specific for claudin-1 is labeled with Cy5.5, a near-infrared fluorophore, and injected intravenously to visualize the molecular expression patterns with subcellular resolution.

MATERIALS AND METHODS

Peptide synthesis and characterization

The peptides were synthesized using a PS3 automatic synthesizer (Protein Technologies Inc, Tucson, AZ) and labeled with Cy5.5, a near-infrared red (NIR) fluorophore (cyanine5.5 NHS ester, #27020; Lumiprobe, Hunt Valley, MD), on the C-terminus using a GGGSK linker (14). The peptides were purified to >99% by HPLC and lyophilized for storage at −80 °C.

Animal model

All animal experiments were performed with approval from the University Committee on the Use and Care of Animals at Michigan Medicine. Mice were housed (2–4/cage) in specific-pathogen-free facility, given a standard chow diet and water ad libitum, and exposed to a 12-hour light/12-hour dark cycle. Chlorophyll-free chow diet (ENVIGO TD.97184) was provided 1 week before imaging to minimize autofluorescence background. *CPC;Apc* mice (CDX2-Cre; $Apc^{580S/+}$) were generated by crossing CDX2P 9.5-NLS Cre mice with mice carrying 2 loxP-flanked Apc alleles (ApcloxP/loxP, 580S). The CDX2P9.5 fragment was expressed throughout the caudal region of the embryo and was restricted to the terminal ileum, cecum, and colon in adult tissues. *CPC;Apc* mice express a truncated Apc allele in the colon that results in spontaneous development of adenomas (22).

Claudin-1 expression with wide-field endoscopy

A rigid wide-field endoscope (Karl Storz Veterinary Endoscopy-America, Goleta, CA) was inserted into the distal colon of *CPC;Apc* mice at 2–4 months of age. Before imaging, the mice were fasted for 4–6 hours. Feces and mucus were removed by rinsing the colon with water. Anesthesia was induced and maintained through a nose cone with inhaled isoflurane mixed with oxygen at concentrations of 2%–4% at a flow rate of 0.5 L/min (14). The peptide was administrated intravenously at a concentration of 200 μM in 200 μL of phosphate-buffered saline (PBS). This instrument was adapted to provide excitation at λ_{ex} = 671 nm (23). Images were collected from 0 to 24 hours after peptide injection. A ratio of fluorescence and coregistered reflectance images was determined to correct for differences in distance and geometry over the field-of-view (24). A total of 3 independent regions with dimensions of 20 × 20 μm^2 were identified randomly from the location of the adenoma (target) and from adjacent normal colonic mucosa (background). The mean fluorescent intensity was used to calculate the target-to-background (T/B) ratio. Images were processed and analyzed using custom software in Matlab (MathWorks, Natick, MA).

Claudin-1 expression with confocal endomicroscopy

A confocal endomicroscope with side-view optics having a working distance = 100 μm was used to visualize the mucosal expression pattern of claudin-1 *in vivo* with subcellular resolution (20). Excitation was provided at λ_{ex} = 660 nm. Fluorescence emission centered at λ_{em} = 720 nm was collected with 0.05 sec exposure time. A group of n = 9 *CPC;Apc* mice with a total of n = 9 adenomas was imaged at ~1 hour after intravenous injection of peptide at a concentration of 200 μM in 200 μL of PBS. Images were processed and analyzed using custom Matlab software. Briefly, the average fluorescence intensity was determined from 3 independent regions of interest with dimensions of 20 × 20 pixels in each image that represent a range of intensities for adenoma and adjacent normal mucosa. Free Cy5.5 was dissolved in PBS at a concentration of 200 μM and then injected intravenously at a volume of 200 μL per mouse. Confocal images were collected at ~10 minutes after injection. Fluorescein (FX0325; EMD Millipore, Burlington, MA) was dissolved in PBS at 5% concentration and then injected intravenously at a volume of 200 μL per mouse. Excitation was provided at λ_{ex} = 488 nm, and emission centered at λ_{em} = 532 nm was collected.

Validation of claudin-1 expression *ex vivo*

Immunofluorescence. Immunofluorescence (IF) was performed to validate claudin-1 expression *ex vivo*. The distal colon was divided, opened longitudinally, and rinsed with cold PBS. The tissues were fixed in 10% neutral-buffered formalin for ~48 hours and then transferred into 70% ethanol. The tissues were processed for routine histology (H&E). Deparaffinization and antigen retrieval were performed on adjacent, unstained sections, as described previously (14). For peptide staining, the sections were blocked with 2% bovine serum albumin (BSA) for ~1 hour and 0.5 μM of peptide for 10 minutes. For antibody staining, blocking was performed using 10% normal serum followed by ~1 hour of incubation with either anti–claudin-1 (#15098; Abcam, Cambridge, MA) or anti–β-catenin antibody (#16051; Abcam, Cambridge, MA). Goat anti-rabbit IgG antibody conjugated with either AF488 (#A-11029; Life Technologies, Carlsbad, CA) or AF647 (#205-605-108; Jackson, West Grove, PA) was used. For colocalization of RTS*-Cy5.5 and anti–claudin-1 antibody staining, the tissues were incubated with peptide first for 10 minutes followed by goat anti-rabbit IgG antibody conjugated with AF488 (#A-11029; Life Technologies, Carlsbad, CA). Fluorescence images were collected using an inverted confocal microscope (Leica inverted SP5).

Western blot analysis. Western blot was performed by rinsing the fresh tissues in ice cold PBS and collecting in RIPA buffer containing phosphatase and protease inhibitors. The tissues were homogenized immediately, and the proteins were extracted after incubation on ice for ~30 minutes. The total protein concentration was measured using a Pierce BCA Protein Assay kit (#23225; ThermoFisher Scientific, Waltham, MA) per manufacturer instructions. Western blot analysis was performed using diluted protein samples (4 μg/μL). Briefly, 80 μg of protein was separated on 4%–12% Bis-Tris gel and transferred onto a 0.22-μm polyvinylidene fluoride (PVDF) membrane. After ~1 hour for blocking with 5% nonfat milk, the membrane was incubated with either anti–claudin-1 antibody at 1:250 dilution (#15098; Abcam, Cambridge, MA) or anti–β-actin antibody at 1:500 dilution (#4967s; Cell Signaling, Danvers, MA) for ~2 hours, washed in 1× Tris-Buffered Saline with 0.1% Tween 20 (TBST), and then incubated with horseradish peroxidase (HRP)-conjugated goat-anti-rabbit IgG antibody for another ~2 hours. HRP signal was detected using the Pierce ECL western blotting substrate (#32106; ThermoFisher Scientific, Waltham, MA) per manufacturer protocol.

Reverse transcription polymerase chain reaction (RT-PCR). Gene expression of claudin-1 was performed by isolating RNA from whole tissues using a Direct-zol RNA kit (Zymo Research, Irvine, CA). Single-stranded cDNA was transcribed from purified RNA using a high-capacity cDNA reverse transcription kit (#4368814; ThermoFisher Scientific). Each 10 μL of RNA produces ~20 μL of concentrated cDNA per manufacturer protocol. All cDNA samples were diluted in 80 μL of nuclease-free water and stored at −80 °C. cDNA was analyzed using RT-PCR. Primer sets (Intergrated DNA Technologies, Coralville, IA) with the following assay IDs were used: Actb (Mm.PT.39a.22214843.g), Ctnnb1 (Mm.PT.58.12501105), Cldn1 (Mm.PT.58.6163880), Myc (Mm.PT.58.13590978), and Ccnd1 (Mm.PT.58.28503828). Actb is used as a house-keeping gene. PCR was performed using the PrimeTime Gene Expression Master Mix (Intergrated DNA Technologies) with the following cycling conditions: 95 °C for 3 minutes and then 40 cycles at 95 °C for 15 seconds and 60 °C for 30 seconds. Relative expression levels were determined by using the delta delta Ct method (25).

Immunohistochemistry. Immunohistochemistry (IHC) was performed to confirm the IF results using the same specimens. Tissue specimens were incubated with 3% H_2O_2 for 30 minutes, blocked with normal serum for 30 minutes, and incubated with either anti–claudin-1 or anti–β-catenin rabbit polyclonal antibody for 60 minutes. Antigen binding was detected using a Vectastain Elite ABC HRP kit containing biotinylated rabbit IgG (#PK6101), mouse IgG (#PK6102), and chromogen 3,3'-diaminobenzidine (DAB; #D3939, Sigma, St. Louis, MO) per manufacturer's instructions. The sections were counterstained with Harris hematoxylin.

Peptide pharmacokinetics and safety

Serum stability. The peptides were dissolved in sterile PBS at a concentration of 200 μM in 200 μL and were injected intravenously in C57BL6/J mice (n = 3). Serum was collected from the tail vein from 0 to 48 hours after injection. The fluorescence intensity for each time point was measured (Pearl; LI-COR Biosciences, Lincoln, NE). The data were fit to a first-order kinetics model $y = y_0 + A \times \exp(B \times t)$ (OriginLab) (26). For high performance liquid chromatography (HPLC), the peptides at a concentration of 30 uM were incubated in mouse serum at 37 °C for up to 24 hours. The samples were centrifuged at 14,000 rpm, and 20-μL aliquots of the supernatant are analyzed by HPLC at each time point (27).

Biodistribution. *CPC;Apc* mice were injected intravenously with 200 μL of PBS containing 200 μM of either peptide or Cy5.5. The animals were sacrificed at ~1 hour after injection. Major organs were collected, rinsed in cold PBS, dried, and placed on a black card for imaging without perfusion. Fluorescence images were collected using the IVIS spectrum (PerkinElmer, Waltham, MA). Excitation was provided at λ_{ex} = 640 nm, and fluorescence emission was collected at λ_{em} = 720 nm. Images were analyzed using Living Images, ver 4.5.1, software. Three independent regions were used to measure the fluorescence intensity from each organ and averaged.

Pathology. Acute toxicity was evaluated by injecting 200 μM of peptide diluted in 200 μL of PBS in *CPC;Apc* mice. All mice were visually inspected daily for general health, including food intake, water consumption, and movement. The animals were euthanized on day 7 after injection, and major organs, including the brain, heart, liver, spleen, lung, kidney, and colon, were evaluated for necropsy. The tissues were processed for routine histology (H&E) and evaluated by an expert pathologist (H.D.A.).

Statistics

Fluorescence intensities from *in vivo* images were log-transformed and analyzed using paired *t* tests. IF results were fit into an ANOVA model followed by pairwise comparisons. For gene expression, each transcript was fit to an individual ANOVA model, and pairwise comparisons were performed. IF intensities were log-transformed and analyzed using paired *t* tests. Biodistribution data were log-transformed and fit to an ANOVA model.

RESULTS

Claudin-1 peptide characterization and pharmacokinetics

The 7mer peptide RTSPSSR was covalently linked to Cy5.5 through a GGGSK linker, hereafter RTS*-Cy5.5. The sequence was scrambled as SPTSSRR for use as control; hereafter, SPT*-Cy5.5. 3D biochemical structures of RTS*-Cy5.5 and SPT*-Cy5.5 are shown, Figure 1a,b. A rigid small animal endoscope was used to visualize the mucosal surface in the distal colon of *CPC; Apc* mice. White light illumination was used first to identify the presence of adenomas (see video, Supplemental Digital Content 1, http://links.lww.com/CTG/A135). The distance between the endoscope tip and the anus and the clockwise location of adenomas was recorded for use as landmarks. Autofluorescence background was minimal. After intravenous injection of RTS*-Cy5.5, NIR fluorescence and reflectance images were collected concurrently at 0.5, 1, 2, 4, 7, 10, and 24 hours to visualize claudin-1 expression patterns (see video, Supplemental Digital Content 2, http://links.lww.com/CTG/A136, Supplemental Digital Content 3, http://links.lww.com/CTG/A137). The same mice were injected with SPT*-Cy5.5 (control) 1 week later after all signal from RTS*-Cy5.5 had cleared. A significant reduction in intensity was seen (see video, Supplemental Digital Content 4, http://links.lww.com/CTG/A138). Peak uptake of RTS*-Cy5.5 was observed at ~1 hour, and the T/B ratio returned to baseline by 24 hours, Figure 1c.

Serum stability

Fluorescence was collected from mouse serum at various time points after *in vivo* administration of RTS*-Cy5.5 to evaluate

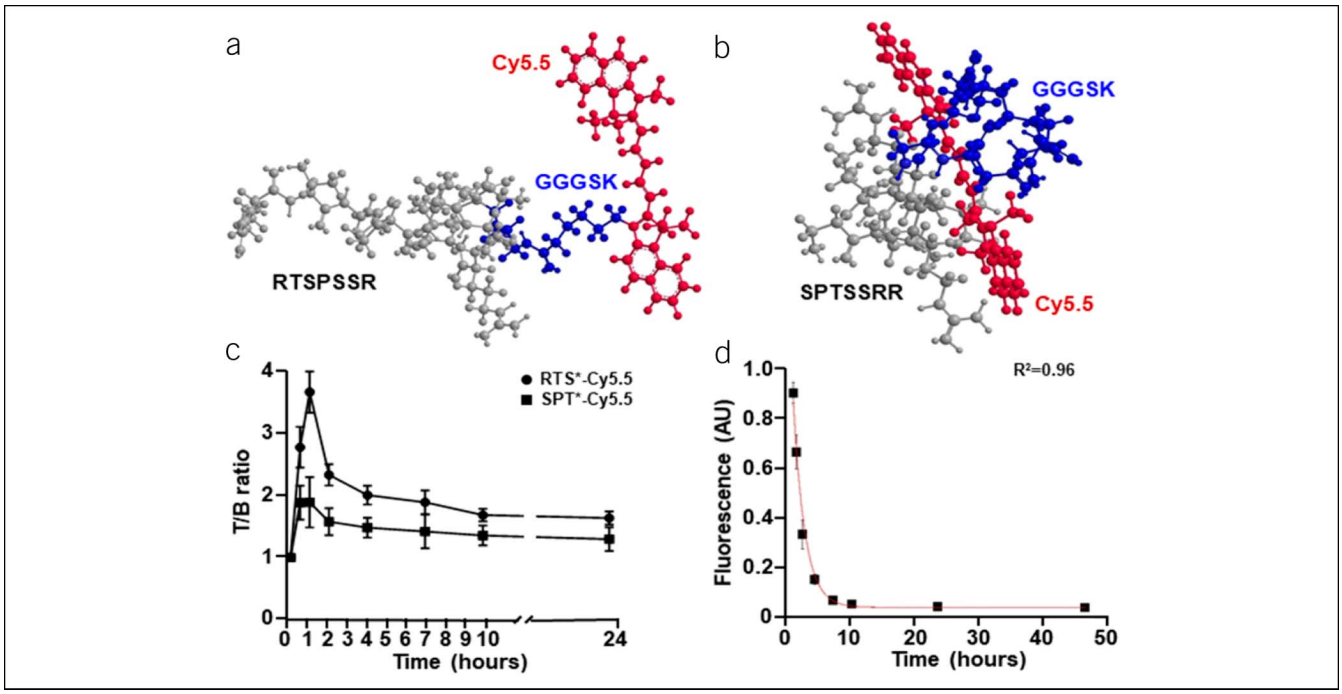

Figure 1. Claudin-1 peptide characteristics. 3-dimensional (3D) structures for (**a**) RTS*-Cy5.5 and (**b**) SPT*-Cy5.5 are shown. (**c**) Peak uptake of RTS*-Cy5.5 is observed at ~1 hour after injection, and signal returns to baseline by ~24 hours (n = 11 mice). (**d**) Fluorescence intensities measured from RTS*-Cy5.5 in mouse serum at 37 °C show $T_{1/2}$ = 1.9 hours from fit to a first-order kinetics model (n = 3 mice).

stability (see Figure, Supplemental Digital Content 5A, http://links.lww.com/CTG/A139). The intensities were fit to a first order kinetic model, and a half-life of $T_{1/2}$ = 1.9 hours was estimated, Figure 1d. RTS*-Cy5.5 was incubated in mouse serum at 37 °C *ex vivo* and evaluated using HPLC at 0, 1, and 2 hours to support peptide stability (see Figure, Supplemental Digital Content 5B-D, http://links.lww.com/CTG/A139). The results at 24 hours show signs of peptide breakdown (see Figure, Supplemental Digital Content 5E, http://links.lww.com/CTG/A139).

Claudin-1 expression with wide-field endoscopy

A representative white light image collected from a nonpolypoid adenoma (arrow) is shown, Figure 2a, Video, Supplemental Digital Content 6, http://links.lww.com/CTG/A140. Coregistered fluorescence and reflectance images were collected, Figure 2b,c (see video, Supplemental Digital Content 7, http://links.lww.com/CTG/A141, Supplemental Digital Content 8, http://links.lww.com/CTG/A142) and ratioed to correct for differences in distance and geometry over the image field-of-view. The ratio image showed the location of the nonpolypoid adenoma in pseudocolor (see Figure, Supplemental Digital Content 9A, http://links.lww.com/CTG/A143). Fluorescence, reflectance, and ratio intensities from the dashed line in Supplemental Digital Content 9A, http://links.lww.com/CTG/A143 are shown in Supplemental Digital Content 9B, http://links.lww.com/CTG/A143. After signal from RTS*-Cy5.5 cleared 1 week later, NIR fluorescence images were collected from the nonpolypoid adenoma after intravenous administration of SPT*-Cy5.5, and minimal signal was seen, Figure 2d (see video, Supplemental Digital Content 10, http://links.lww.com/CTG/A144). A representative white light image collected from a polypoid adenoma (arrow) is shown, Figure 2e. Coregistered fluorescence and reflectance images were collected and ratioed, Figure 2f,g. The ratio image highlights the location of the polypoid adenoma in pseudocolor (see Figure, Supplemental Digital Content 9C, http://links.lww.com/CTG/A143). Fluorescence, reflectance, and ratio intensities from dashed line in Supplemental Digital Content 9C, http://links.lww.com/CTG/A143 are shown in Supplemental Digital Content 9D, http://links.lww.com/CTG/A143. Fluorescence images collected from the polypoid adenoma after intravenous administration of SPT*-Cy5.5 showed minimal signal, Figure 2h. The mean T/B ratio was significantly greater for RTS*-Cy5.5 than for SPT*-Cy5.5 for nonpolypoid and polypoid adenomas at ~1 hour after injection, Figure 2i,j.

Claudin-1 expression with confocal endomicroscopy

A confocal endomicroscope was used to visualize claudin-1 expression with subcellular resolution *in vivo* (20). Landmarks identified with wide-field endoscopy were used to position the side-view optics for contact with the mucosa. Premalignant crypts from an adenoma showed strong binding by RTS*-Cy5.5 to the cell surface, Figure 3a, Video, Supplemental Digital Content 11, http://links.lww.com/CTG/A145. These crypts are structurally large in size, elongated in shape, distorted in architecture, and variable in dimension, and the lamina propria appears crowded. Normal crypts show binding at tight junctions in between cells, Figure 3b, Video, Supplemental Digital Content 12, http://links.lww.com/CTG/A146, and appear oval in shape with similar dimensions. SPT*-Cy5.5 produced a nonspecific staining pattern in adenoma, Figure 3c, and a vague appearance of crypt structures in normal colon, Figure 3d. The mean fluorescence intensity was significantly

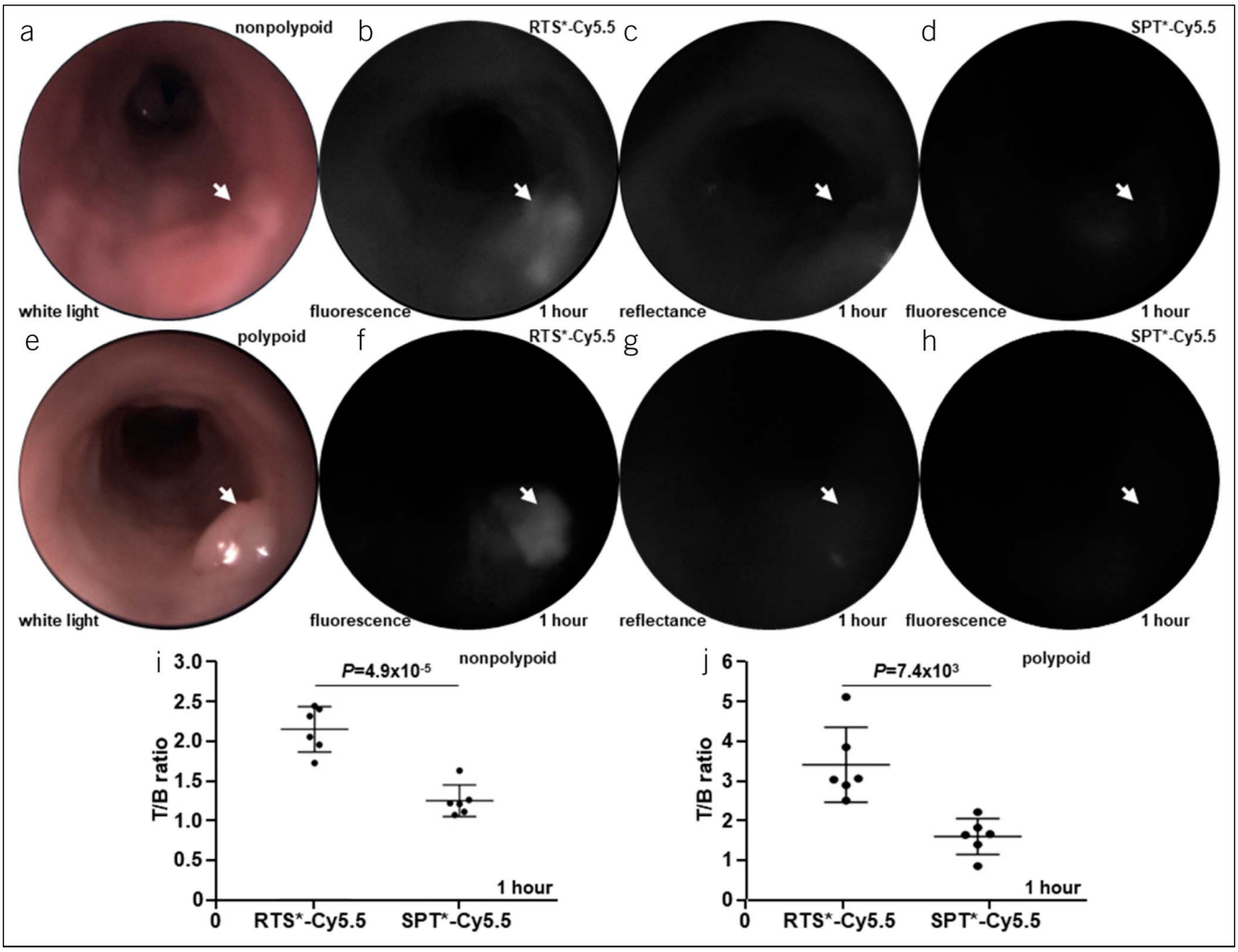

Figure 2. Claudin-1 expression with wide-field endoscopy. (**a**) White light image is shown of nonpolypoid lesion in mouse colon (arrow). (**b**) NIR fluorescence image of RTS*-Cy5.5 shows increased intensity from nonpolypoid lesion (arrow) at ~1 hour after intravenous administration. (**c**) Reflectance image collected is coregistered with fluorescence. (**d**) Image from SPT*-Cy5.5 (control) is collected from the same animal 7 days later after signal from RTS*-Cy5.5 has cleared. (**e**–**h**) White light, fluorescence (RTS*-Cy5.5), reflectance, and fluorescence (SPT*-Cy5.5) images of a polypoid lesion are shown. (**i**, **j**) The mean (±SD) T/B ratios for RTS*-Cy5.5 vs SPT*-Cy5.5 with nonpolypoid and polypoid adenomas are shown. Image intensities were log-transformed and analyzed with paired *t* tests, n = 6 mice per group. NIR, near-infrared red.

greater for adenoma than for adjacent normal colon with RTS*-Cy5.5 at ~1 hour after injection, Figure 3e, and the mean T/B ratio was significantly greater for RTS*-Cy5.5 than for SPT*-Cy5.5 in adenoma at ~1 hour, Figure 3f. Free Cy5.5 and fluorescein (without peptide) were injected intravenously, and the confocal images showed nonspecific uptake of dye in the lamina propria (lp) (see Figure, Supplemental Digital Content 13, http://links.lww.com/CTG/A147).

Biodistribution

Uptake of RTS*-Cy5.5, SPT*-Cy5.5, and Cy5.5 in the major organs of *CPC;Apc* mice at ~1 hour after injection is shown, Figure 4a–c. The mean fluorescence intensity is significantly greater for RTS*-Cy5.5 than for SPT*-Cy5.5 and Cy5.5 in adenoma to confirm the *in vivo* findings, Figure 4d. Also, the result is significantly higher for adenoma than for adjacent normal colon. The strong fluorescence intensity from the kidney and liver is likely from peptide clearance by the reticuloendothelial system, while the signal from the lungs is likely from nonspecific uptake.

Ex vivo validation

Peptide staining is performed *ex vivo* to validate the *in vivo* results. Increased binding of RTS*-Cy5.5 to premalignant colonocytes is seen in adenoma, Figure 5a. Binding of RTS*-Cy5.5 to tight junctions in between colonocytes is observed in normal crypts, Figure 5b. Minimal signal is seen with SPT*-Cy5.5 (control) for both adenoma and normal colon, Figure 5c,d. The mean fluorescence intensity is significantly greater for adenoma vs normal with RTS*-Cy5.5 and for RTS*-Cy5.5 vs SPT*-Cy5.5 in adenoma, Figure 5e. No difference is found with SPT*-Cy5.5. Representative histology (H&E) is shown for adenoma and normal mouse colon, Figure 5f,g. Costaining of RTS*-Cy5.5 and anti–claudin-1 antibody resulted in a correlation of $\rho = 0.66$ for adenoma and $\rho = 0.60$ for

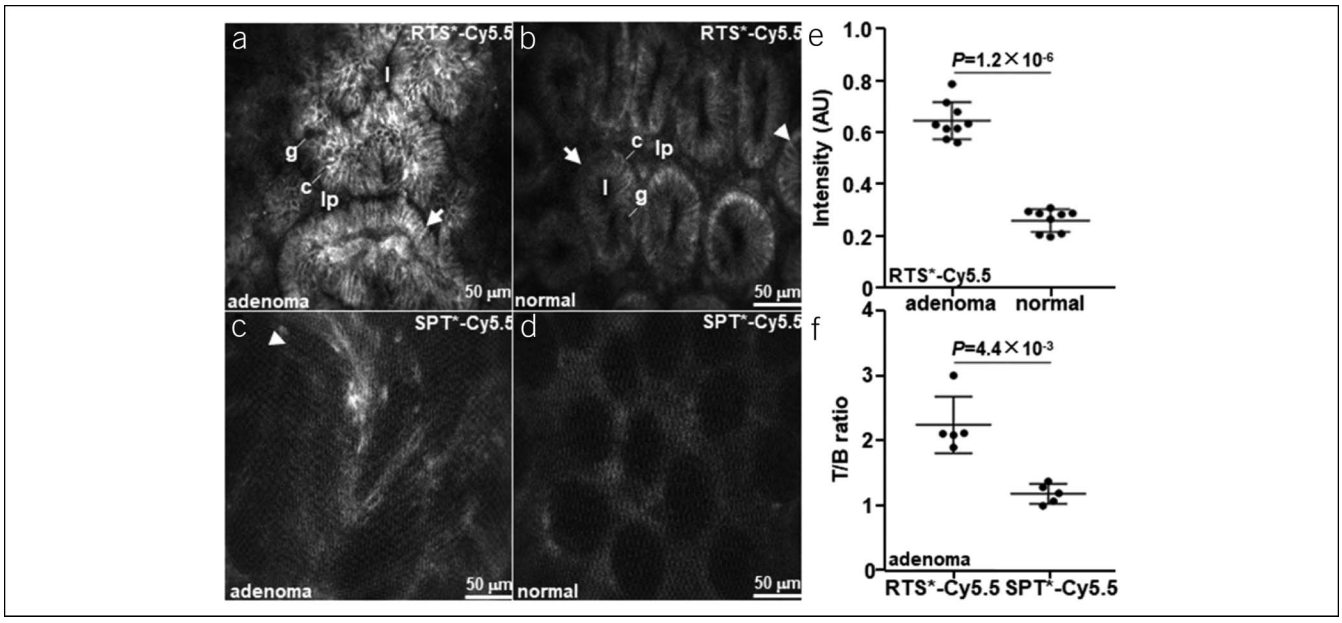

Figure 3. Claudin-1 expression with confocal endomicroscopy. *In vivo* images are shown from (**a**) adenoma and (**b**) normal colon at ~1 hour after injection of RTS*-Cy5.5. Crypt structures and individual cells can be identified. Images of (**c**) adenoma and (**d**) normal colon after injection of SPT*-Cy5.5 are shown. (**e**) The mean (±SD) fluorescence intensity is significantly greater for adenoma vs normal with RTS*-Cy5.5 (n = 11 mice). (**f**) The mean (±SD) T/B ratio is significantly greater for RTS*-Cy5.5 vs SPT*-Cy5.5 in adenomas (n = 5 mice). Image intensities were log-transformed and analyzed with paired *t* tests. Key: crypt (arrow), tight junction (arrowhead), lumen (l), colonocyte (c), goblet cell (g), and lamina propria (lp).

normal (see Figure, Supplemental Digital Content 14, http://links.lww.com/CTG/A148).

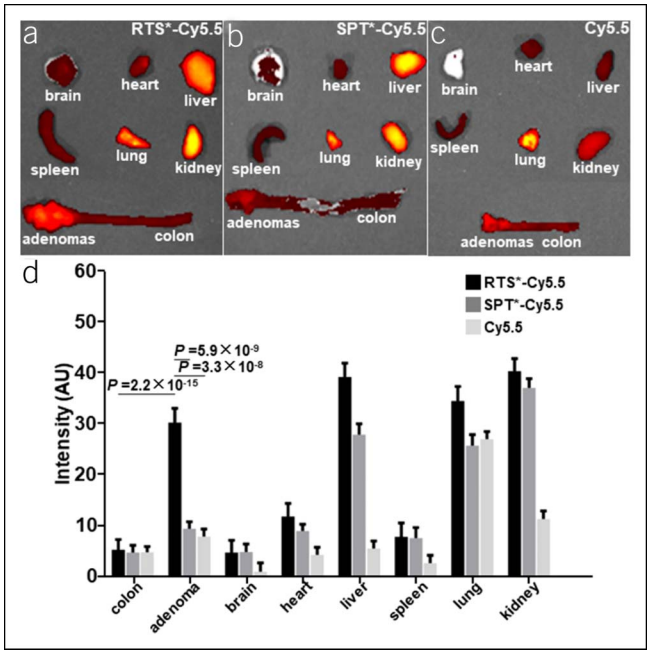

Figure 4. Biodistribution of claudin-1 peptide. Fluorescence images show uptake of (**a**) RTS*-Cy5.5 (n = 6), (**b**) SPT*-Cy5.5 (n = 6), and (**c**) free Cy5.5 (n = 3) in major organs of *CPC;Apc* mice at ~1 hour after injection. (**d**) The mean (±SD) fluorescence intensity is significantly greater for RTS*-Cy5.5 vs either SPT*-Cy5.5 or Cy5.5 in adenoma and for adenoma vs normal colon with RTS*-Cy5.5. Intensities were log-transformed and fit to an ANOVA model using terms for 24 means (3 groups, 8 tissues) and mouse effects.

Transcriptional activity of claudin-1 in adenomas

RT-PCR was performed to evaluate gene expression and support increased transcriptional activity of claudin-1 in adenoma vs normal colon. The mean levels for β-catenin and downstream c-myc and cyclin D1 were found to be significantly greater for adenoma vs adjacent normal colon (distal and proximal) and for small bowel from *CPC;Apc* mice, Figure 6a,b. Claudin-1 (CLDN1) is expressed at significantly higher levels in adenoma. Increased protein expression of CLDN1 in adenomas was confirmed using western blot, Figure 6c. Higher levels of β-catenin, Figure 6d,e, and CLDN1, Figure 6f,g, were seen in adenoma vs normal colon using IHC. IF with RTS*-Cy5.5 (red) and anti–Cldn1-AF488 (green) confirms greater levels of β-catenin and CLDN1 expression in adenoma vs normal colon, Figure 6h–k. The mean fluorescence intensity for β-catenin and CLDN1 was significantly greater for adenomas vs normal, Figure 6l,m.

Pathology

Acute toxicity with a single dose of RTS*-Cy5.5 was evaluated in n = 6 *CPC;Apc* mice. All mice appeared healthy by visual inspection before injection and survived to the scheduled necropsy. The animals were euthanized at day 7 after injection, and anatomic pathology of the brain, heart, liver, spleen, lung, kidney, normal colon, and adenoma was performed. An expert pathologist (H.D.A.) examined all specimens and found no sign of test article-related toxicity at terminal necropsy (see Figure, Supplemental Digital Content 15, http://links.lww.com/CTG/A149).

DISCUSSION

A targeted imaging strategy is demonstrated that combines wide-field endoscopy with confocal endomicroscopy to visualize claudin-

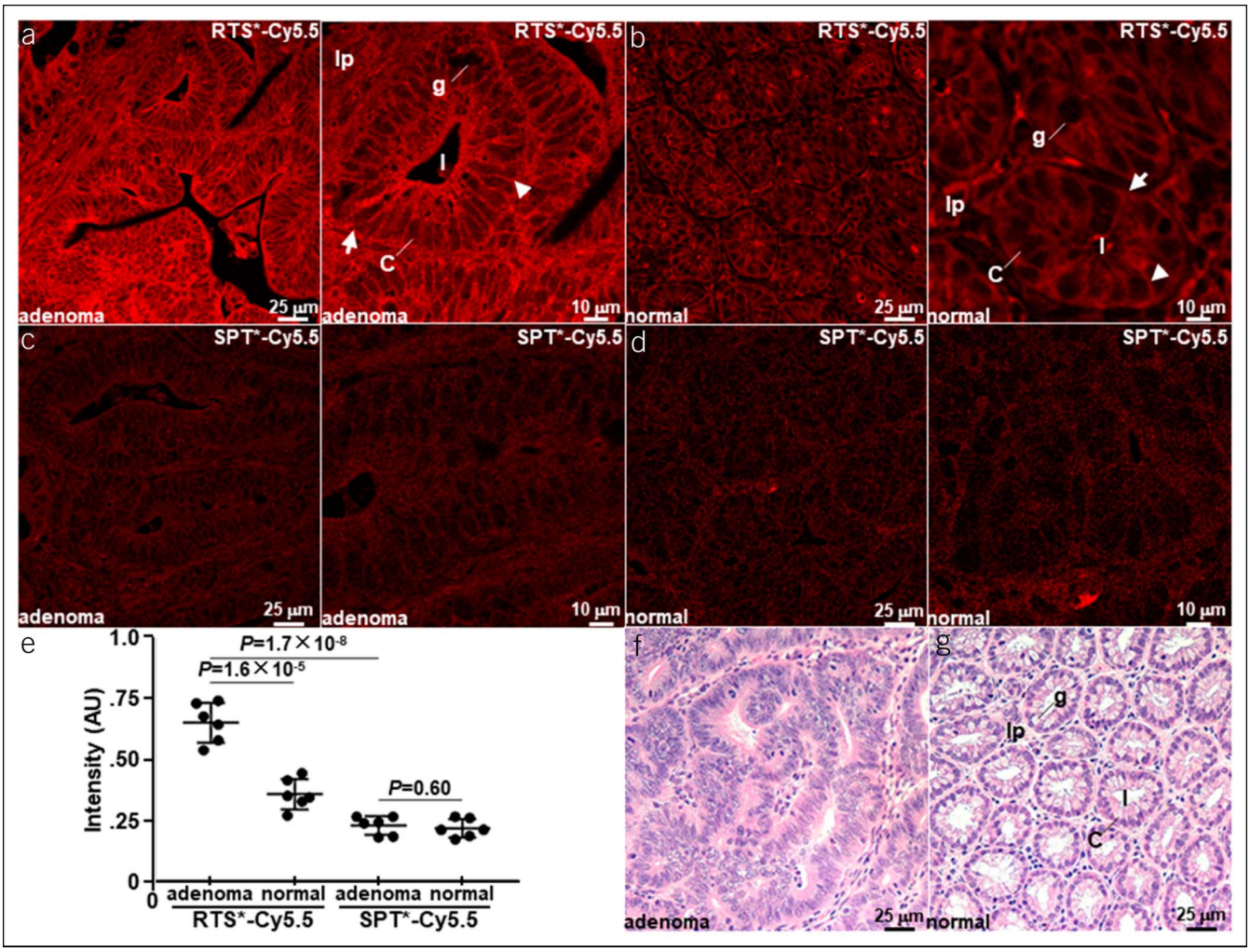

Figure 5. *Ex vivo* validation of claudin-1 expression. Staining of (**a**) adenoma and (**b**) normal mouse colon with RTS*-Cy5.5 shows binding to the cell surface (arrow) at tight junctions (arrowhead). Minimal signal is seen with SPT*-Cy5.5 (control) in (**c**) adenoma and (**d**) normal. (**e**) Quantified results show significantly greater mean (±SD) intensity for adenomas vs normal with RTS*-Cy5.5 and for RTS*-Cy5.5 vs SPT*-Cy5.5 with adenomas. The adenoma vs normal difference is significantly greater for RTS*-Cy5.5 than the same difference for SPT*-Cy5.5 ($P = 1.1 \times 10^{-3}$). Image intensities were log-transformed and analyzed with paired *t* tests, n = 6 per group. Representative histology (H&E) is shown for (**f**) adenoma and (**g**) normal. Key: crypt (arrow), tight junction (arrowhead), lumen (l), colonocyte (c), goblet cell (g), and lamina propria (lp).

1 expression *in vivo* in a mouse model of CRC. This integrated approach provides a strategy to image cancer biomarkers on the macroscopic and microscopic scale in real time. Wide-field endoscopy was performed to localize regions of specific binding by a fluorescently labeled peptide over large mucosal surface areas. These images were used to guide placement of a side-view confocal instrument to validate presence of premalignant epithelium with subcellular resolution. The peptides were injected intravenously, and peak uptake was observed ~1 hour later. Peptide stability in mouse serum was found to have a half-life of $T_{1/2}$ = 1.9 hours. This result was confirmed using HPLC. Fluorescence images collected *ex vivo* validated the *in vivo* results. No evidence of acute peptide toxicity was found in animal necropsy studies.

White light colonoscopy is used widely for CRC screening (28), but effectiveness is limited by a high adenoma miss rate (29,30). Advanced imaging methods are being developed to improve diagnostic performance. Chromoendoscopy is based on topical administration of intravital dyes, such as indigo carmine, methylene blue, and acetic acid, to highlight epithelial abnormalities associated with premalignant lesions (31), and has been recommended by GI societies for cancer surveillance in patients with inflammatory bowel disease (32). Techniques of "virtual" chromoendoscopy incorporate either optical or electronic modifications to the light filtering scheme to enhance these patterns. These technologies include narrow-band imaging, autofluorescence imaging, Fujinon intelligent chromoendoscopy, and i-SCAN (33–36). However, all these approaches are based on nonspecific contrast mechanisms rather than the molecular processes that drive cancer progression. Results of clinical studies using these technologies have not shown a clear advantage over conventional colonoscopy in terms of patient outcomes.

Wide-field imaging methods are being developed for clinical use based on exogenous agents that generate specific contrast using fluorescence. Bevacizumab binds specifically to vascular

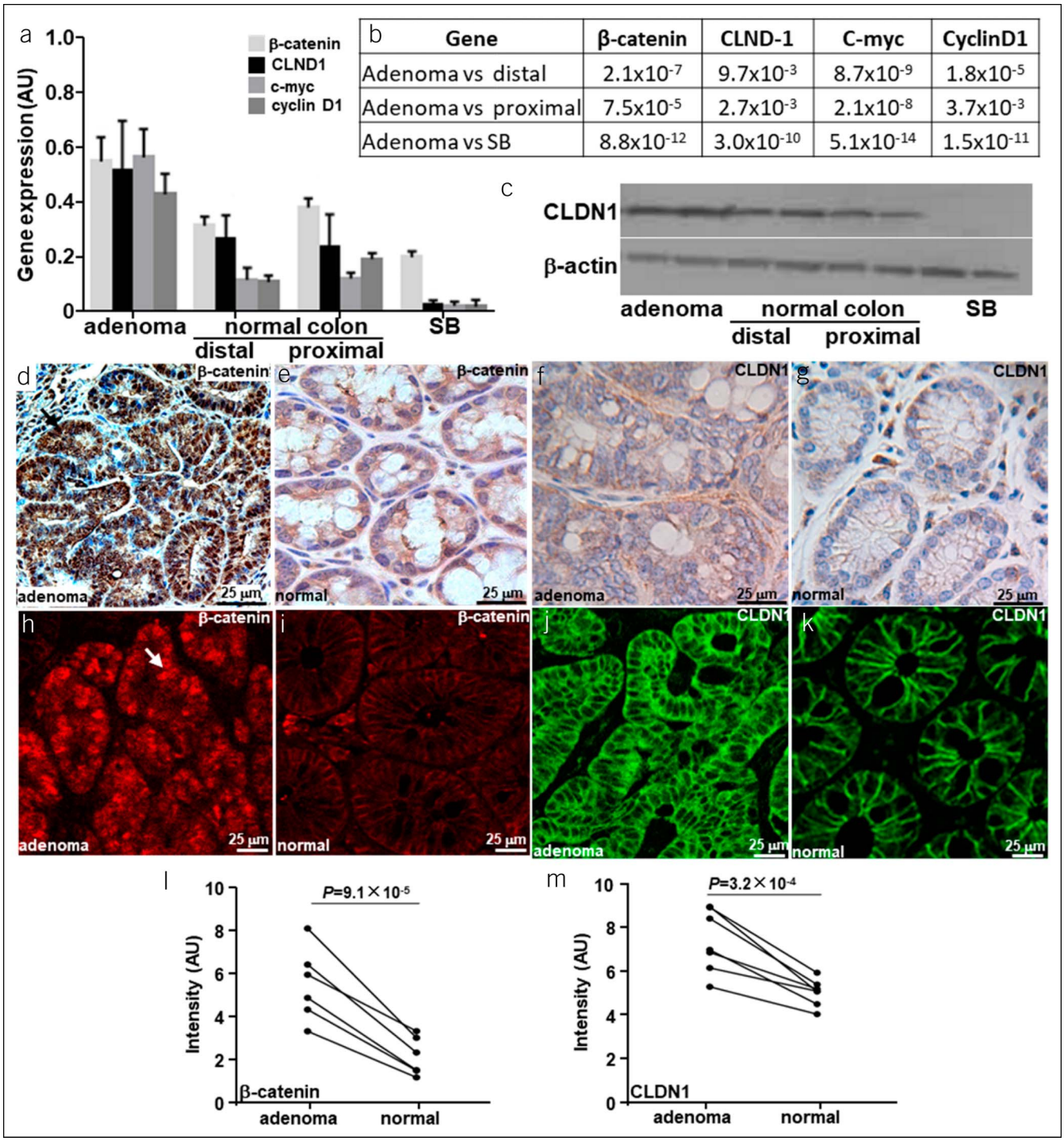

Figure 6. Regulation of claudin-1 expression. (**a**) Mean (±SD) gene expression of β-catenin, claudin-1 (CLDN1), c-myc, and cyclin D1 is increased in adenoma vs either normal colon (proximal and distal) or small bowel (SB) using RT-PCR. (**b**) *P* values are shown for each comparison. (**c**) Western blot confirms increased claudin-1 expression in adenoma vs normal colon and SB. Strong reactivity for β-catenin is seen in the nuclei (arrow) of (**d**) adenoma vs (**e**) normal with immunohistochemistry (IHC), and increased staining for CLDN1 is seen on the membrane of adenoma (**f**) vs normal (**g**). (**h–k**) These results are supported using immunofluorescence and for claudin-1. The mean (±SD) intensities for (**l**) anti–β-catenin and (**m**) anti-CLDN1 antibodies are significantly greater for adenoma vs normal using the paired *t* test, n = 6 per group.

endothelial growth factor A and has been repurposed for *in vivo* imaging (37). This monoclonal antibody has been labeled with IRDye800, an NIR fluorophore, and was injected intravenously in n = 17 patients with familial adenomatous polyposis. Small adenomas <3 mm were detected using a 25-mg dose, and an average T/B ratio of 1.84 was achieved. A peptide specific for c-Met was labeled with Cy5 and administered systemically in n = 15 patients at high risk of CRC (13). NIR fluorescence

colonoscopy was performed, and all polyps grossly visible with white light illumination were seen with fluorescence as well. In addition, n = 9 adenomas missed with white light were detected with fluorescence. A peptide labeled with fluorescein was topically administered in n = 18 patients undergoing routine colonoscopy (38). A flexible fiber confocal endomicroscope was passed through the instrument channel of the colonoscope and was used to collect *in vivo* images to validate specific peptide binding to dysplastic colonocytes.

Confocal laser endomicroscopy has been used to detect a variety of pathologies in the colon, including neoplasia, inflammation, and infection (39–42). Fluorescein was administrated intravenously to improve contrast for visualization. Although the images collected showed structural differences between normal and diseased mucosa, the background was high, and dye uptake was nonspecific. RTS*-Cy5.5 was developed to bind specifically to claudin-1 and is used to highlight tight junctions between the membranes of colonic epithelial cells. Nonspecific signal from the lamina propria and cytoplasm is limited, and subcellular structures are more clearly visualized. Also, claudin-1 is highly overexpressed in neoplasia and can serve as an early biomarker for CRC transformation. IHC and IF results supported the increased activity of transcription factor β-catenin to stimulate claudin-1 expression. *In vivo* imaging of the small bowel was not performed because the rigid instruments used cannot reach this region of the bowel in mice.

Further development of this imaging technology is needed before clinical translation. Peptides have poor oral availability; thus, this contrast agent must be administered intravenously for adequate distribution through all segments of colon. Although a serum half-life of ~2 hours is short by comparison with that for antibodies, this duration is adequate to complete a colonoscopy procedure. Chemical modifications can be made to improve serum stability, including use of D-amino acids, nonnatural amino acids, PEGylation, and N- and C-terminus modifications (43–45). Background can be reduced by using a NIR rather than visible fluorophore to label the peptide. Although no acute toxicity was observed in a limited animal necropsy study, a more rigorous toxicology study should be performed to establish preclinical safety before human use. The preclinical results shown in this study demonstrate promise for an integrated imaging strategy to target molecular changes in premalignant colonic epithelium to improve methods for early CRC detection.

CONFLICTS OF INTEREST

Guarantor of the article: Thomas D. Wang, MD, PhD.

Specific author contributions: F.W. and T.D.W.: study concept and design. F.W., X.D., J.C., Z.G., X.W., and G.L.: acquisition of data. F.W., X.D., M.L., T.C., J.Z., R.K., A.N., H.A., and T.D.W.: analysis and interpretation of data. F.W. and T.D.W.: drafting of manuscript.

Financial support: Funding was provided in part by R01 CA193377 (T.D.W.) and P30 CA046952 (R.K.). The authors thank Haijun Li, Xue Li, Quan Zhou, Shuling Fan, and Ying Feng for technical support.

Potential competing interests: T.D.W. is an inventor on a patent filed by the University of Michigan on the peptide used in this study. All other authors disclose no conflicts.

Study Highlights

WHAT IS KNOWN

- ✓ Claudin-1 is an integral membrane protein that forms tight junctions between colonic epithelial cells.
- ✓ A fluorescently labeled peptide can bind specifically to claudin-1 *in vivo*.

WHAT IS NEW HERE

- ✓ Expression of claudin-1 at tight junctions in mouse colonic epithelium can be visualized with subcellular resolution *in vivo* using confocal endomicroscopy.
- ✓ Increased expression of claudin-1 reflects activation of the β-catenin pathway activity in a mouse model of colorectal cancer.

TRANSLATIONAL IMPACT

- ✓ Identify sporadic premalignant lesions that appear flat or depressed with conventional white light illumination.
- ✓ Identify premalignant lesions in the setting of inflammatory bowel disease.

REFERENCES

1. Ferlay J, Soerjomataram I, Dikshit R, et al. Cancer incidence and mortality worldwide: Sources, methods and major patterns in GLOBOCAN 2012. Int J Cancer 2015;136(5):E359–386.
2. Slattery ML, Potter JD, Duncan DM, et al. Dietary fats and colon cancer: Assessment of risk associated with specific fatty acids. Int J Cancer 1997; 73(5):670–7.
3. Yang T, Li X, Montazeri Z, et al. Gene-environment interactions and colorectal cancer risk: An umbrella review of systematic reviews and meta-analyses of observational studies. Int J Cancer 2019;145:2315–29.
4. Siegel R, Ma J, Zou Z, et al. Cancer statistics, 2014. CA Cancer J Clin 2014; 64(1):9–29.
5. Zauber AG. The impact of screening on colorectal cancer mortality and incidence: Has it really made a difference? Dig Dis Sci 2015;60(3):681–91.
6. van Rijn JC, Reitsma JB, Stoker J, et al. Polyp miss rate determined by tandem colonoscopy: A systematic review. Am J Gastroenterol 2006; 101(2):343–50.
7. Heresbach D, Barrioz T, Lapalus MG, et al. Miss rate for colorectal neoplastic polyps: A prospective multicenter study of back-to-back video colonoscopies. Endoscopy 2008;40(4):284–90.
8. Park DH, Kim HS, Kim WH, et al. Clinicopathologic characteristics and malignant potential of colorectal flat neoplasia compared with that of polypoid neoplasia. Dis colon rectum 2008;51(1):43–9; discussion 49.
9. Benedict M, Galvao Neto A, Zhang X. Interval colorectal carcinoma: An unsolved debate. World J Gastroenterol 2015;21(45):12735–41.
10. Dong SH, Huang JQ, Chen JS. Interval colorectal cancer: A challenging field in colorectal cancer. Future Oncol 2018;14(13):1307–16.
11. Mahmood U, Weissleder R. Near-infrared optical imaging of proteases in cancer. Mol Cancer Ther 2003;2(5):489–96.
12. Goetz M, Ziebart A, Foersch S, et al. In vivo molecular imaging of colorectal cancer with confocal endomicroscopy by targeting epidermal growth factor receptor. Gastroenterology 2010;138(2):435–46.
13. Burggraaf J, Kamerling IM, Gordon PB, et al. Detection of colorectal polyps in humans using an intravenously administered fluorescent peptide targeted against c-Met. Nat Med 2015;21(8):955–61.
14. Rabinsky EF, Joshi BP, Pant A, et al. Overexpressed claudin-1 can Be visualized endoscopically in colonic adenomas in vivo. Cell Mol Gastroenterol Hepatol 2016;2(2):222–37.
15. Tsukita S, Furuse M. Claudin-based barrier in simple and stratified cellular sheets. Curr Opin Cel Biol 2002;14(5):531–6.
16. Miwa N, Furuse M, Tsukita S, et al. Involvement of claudin-1 in the beta-catenin/Tcf signaling pathway and its frequent upregulation in human colorectal cancers. Oncol Res 2001;12(11-12):469–76.

17. Huo Q, Kinugasa T, Wang L, et al. Claudin-1 protein is a major factor involved in the tumorigenesis of colorectal cancer. Anticancer Res 2009; 29(3):851–7.
18. Dhawan P, Singh AB, Deane NG, et al. Claudin-1 regulates cellular transformation and metastatic behavior in colon cancer. J Clin Invest 2005;115(7):1765–76.
19. Duan X, Li H, Qiu Z, et al. MEMS-based multiphoton endomicroscope for repetitive imaging of mouse colon. Biomed Opt express 2015;6(8): 3074–83.
20. Duan X, Li H, Zhou J, et al. Visualizing epithelial expression of EGFR in vivo with distal scanning side-viewing confocal endomicroscope. Scientific Rep 2016;6:37315.
21. Goetz M, Kiesslich R. Advances of endomicroscopy for gastrointestinal physiology and diseases. Am J Physiol Gastrointest Liver Physiol 2010; 298(6):G797–806.
22. Hinoi T, Akyol A, Theisen BK, et al. Mouse model of colonic adenoma-carcinoma progression based on somatic Apc inactivation. Cancer Res 2007;67(20):9721–30.
23. Liu Z, Miller SJ, Joshi BP, et al. In vivo targeting of colonic dysplasia on fluorescence endoscopy with near-infrared octapeptide. Gut 2013;62(3): 395–403.
24. Joshi BP, Pant A, Duan X, et al. Multimodal video colonoscope for targeted wide-field detection of nonpolypoid colorectal neoplasia. Gastroenterology 2016;150(5):1084–6.
25. Livak KJ, Schmittgen TD. Analysis of relative gene expression data using real-time quantitative PCR and the 2(-Delta Delta C(T)) Method. Methods 2001;25(4):402–8.
26. Chen J, Gao Z, Li G, et al. Dual-modal in vivo fluorescence and photoacoustic imaging using a heterodimeric peptide. Chem Commun 2018;54(94):13196–9.
27. Chen J, Zhou J, Gao Z, et al. Multiplexed targeting of barrett's neoplasia with a heterobivalent ligand: Imaging study on mouse xenograft in vivo and human specimens ex vivo. J Med Chem 2018;61(12):5323–31.
28. Pan J, Xin L, Ma YF, et al. Colonoscopy reduces colorectal cancer incidence and mortality in patients with non-malignant findings: A meta-analysis. Am J Gastroenterol 2016;111(3):355–65.
29. Shin JG, Kim HW, Park SB, et al. Polyp missing rate and its associated risk factors of referring hospitals for endoscopic resection of advanced colorectal neoplasia. Medicine 2017;96(19):e6742.
30. Than M, Witherspoon J, Shami J, et al. Diagnostic miss rate for colorectal cancer: An audit. Ann Gastroenterol 2015;28(1):94–8.
31. Kahi CJ, Anderson JC, Waxman I, et al. High-definition chromocolonoscopy vs. high-definition white light colonoscopy for average-risk colorectal cancer screening. Am J Gastroenterol 2010;105(6):1301–7.
32. Azizi S, Al-Rubaye H, Turki MAA, et al. Detecting dysplasia using white light endoscopy or chromoendoscopy in ulcerative colitis patients without primary sclerosing cholangitis: A systematic review and meta-analysis. Int J Surg 2018;52:180–8.
33. Rex DK, Clodfelter R, Rahmani F, et al. Narrow-band imaging versus white light for the detection of proximal colon serrated lesions: A randomized, controlled trial. Gastrointest Endosc 2016;83(1):166–71.
34. Boerwinkel DF, Holz JA, Kara MA, et al. Effects of autofluorescence imaging on detection and treatment of early neoplasia in patients with Barrett's esophagus. Clin Gastroenterol Hepatol 2014;12(5):774–81.
35. Lami G, Galli A, Macri G, et al. Gastric and duodenal polyps in familial adenomatous polyposis patients: Conventional endoscopy vs virtual chromoendoscopy (fujinon intelligent color enhancement) in dysplasia evaluation. World J Clin Oncol 2017;8(2):168–77.
36. Shan J, Liu L, Sun X, et al. High-definition i-scan colonoscopy is superior in the detection of diminutive polyps compared with high-definition white light colonoscopy: A prospective randomized-controlled trial. Eur J Gastroenterol Hepatol 2017;29(11):1309–13.
37. Tjalma JJ, Garcia-Allende PB, Hartmans E, et al. Molecular fluorescence endoscopy targeting vascular endothelial growth factor A for improved colorectal polyp detection. J Nucl Med 2016;57(3):480–5.
38. Hsiung PL, Hardy J, Friedland S, et al. Detection of colonic dysplasia in vivo using a targeted heptapeptide and confocal microendoscopy. Nat Med 2008;14(4):454–8.
39. Moussata D, Goetz M, Gloeckner A, et al. Confocal laser endomicroscopy is a new imaging modality for recognition of intramucosal bacteria in inflammatory bowel disease in vivo. Gut 2011;60(1):26–33.
40. Kiesslich R, Burg J, Vieth M, et al. Confocal laser endoscopy for diagnosing intraepithelial neoplasias and colorectal cancer in vivo. Gastroenterology 2004;127(3):706–13.
41. Hurlstone DP, Baraza W, Brown S, et al. In vivo real-time confocal laser scanning endomicroscopic colonoscopy for the detection and characterization of colorectal neoplasia. Br J Surg 2008;95(5):636–45.
42. Mielke L, Preaudet A, Belz G, et al. Confocal laser endomicroscopy to monitor the colonic mucosa of mice. J Immunol Methods 2015;421:81–8.
43. Gentilucci L, De Marco R, Cerisoli L. Chemical modifications designed to improve peptide stability: Incorporation of non-natural amino acids, pseudo-peptide bonds, and cyclization. Curr Pharm Des 2010;16(28): 3185–203.
44. Wu H, Huang J. PEGylated peptide-based imaging agents for targeted molecular imaging. Curr Protein Pept Sci 2016;17(6):582–95.
45. Powell MF, Stewart T, Otvos L Jr, et al. Peptide stability in drug development. II. Effect of single amino acid substitution and glycosylation on peptide reactivity in human serum. Pharm Res 1993;10(9):1268–73.